ACS APPLIED MATERIALS & INTERFACES

Research Article

www.acsami.org

Self-Cleaning Organic Vapor Sensor Based on a Nanoporous TiO_2 Interferometer

Fengxia Liang,[†] Timothy L. Kelly,[‡] Lin-bao Luo,[§] Hui Li,[†] Michael J. Sailor,*[,‡] and Yang Yang Li*[,†]

[†]Department of Physics and Materials Science, City University of Hong Kong, Kowloon, Hong Kong SAR, PRC

[‡]Department of Chemistry and Biochemistry, University of California, San Diego, 9500 Gilman Drive, La Jolla, CA 92039-0358, USA

[§]School of Electronic Science and Applied Physics, Hefei University of Technology, Hefei, 230009, Anhui, PRC

Supporting Information

ABSTRACT: Porous thin films of TiO_2 are prepared and their use as chemical sensors for organic vapor analytes is investigated. Thin-film optical interference (Fabry-Perot) fringes in the reflectance spectrum are monitored using Reflectometric Interference Fourier Transform Spectroscopy (RIFTS). Three analytes are employed to probe the sensitivity of the porous TiO_2–based sensors as a function of analyte vapor pressure: dodecane, isopropyl alcohol (IPA), and pentane. Measured lower limits of detection (3, 30, and 11 000 ppmv for dodecane, IPA, and pentane, respectively) track the saturation vapor pressures (P_{sat}) of the analytes (0.134, 45, and 513 Torr at 25°C for dodecane, IPA, and pentane, respectively); the analyte with the lowest value of P_{sat} shows the lowest LLOD. Recovery of the sensor after a saturation dose of analyte is also dependent on P_{sat}: the sensor displays good recovery from pentane and IPA, and sluggish and incomplete recovery from dodecane. However, irradiation of the porous TiO_2 sensor with UV light in the presence of air accelerates recovery, and this process is attributed to photo-catalyzed oxidation of the analyte at the TiO_2 surface.

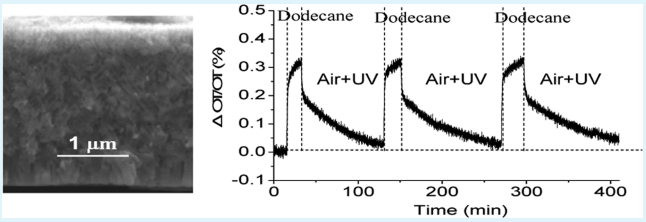

KEYWORDS: *TiO_2, vapor sensor, photocatalysis, porous materials, anodization, optical interference fringes*

INTRODUCTION

Chemical sensors based on optical nanomaterials are of growing interest because of the need for inexpensive, low-power, distributed sensors for application in pollution monitoring, warfighter protection, homeland security, factory worker safety assurance, and food safety.[1,2] A critical limitation of many point sensors is that they become contaminated during long-term exposure to the environment, leading to unacceptable baseline drift and/or loss of sensitivity. Different approaches have been used to refresh sensors intended for long-term monitoring. For example, recovery of contaminated sensors has been demonstrated by application of a gate voltage,[3] by thermal cycling,[4] or by illumination with UV light.[5] This latter method is particularly attractive for optically probed chemical sensors, and it provides the inspiration for the present work.

Because of its inherent advantages such as large surface area, high adsorptivity to organic molecules, non-toxicity, low cost, chemical stability, and the availability of many fabrication methods, TiO_2 nanostructures have been widely studied for sensing applications, e.g., nanostructured TiO_2 networks have been demonstrated for sensing dye molecules.[6] Moreover, because of the photocatalytic activity of this wide bandgap semiconductor, TiO_2 is able to photocatalyze oxidative degradation of a wide range of organic species commonly present in air or water.[7−10] This self-cleaning property makes TiO_2 a very attractive material for use in long-term, unattended chemical sensing applications. The self-cleaning capability of photoexcited TiO_2-based chemical or biological sensors has been demonstrated in several electrical (e.g., resistivity, or capacitance) or optical sensor configurations.[11,12]

The large surface area of porous or nanostructured forms of TiO_2 yields better sensitivity, and various types of TiO_2-based nanomaterials, such as nanoparticles,[13] nanowires,[14] nanobelts,[15] and nanotubes[16,17] have been utilized in chemical sensors. Among the wide range of fabrication methods for TiO_2 nanomaterials, such as hydrothermal, sol−gel, template-assisted, and seed growth methods,[18−21] electrochemical anodization is particularly interesting and widely investigated because of its low cost, ease of fabrication, and the flexibility with which one can fine-tune the nanostructural morphology and specific surface area.[22,23] Prepared by electrochemically anodizing a Ti foil in an acidic electrolyte, this form of TiO_2 has been used in dye-sensitized solar cells,[24] self-cleaning devices,[25] electrochromic optical components,[26] and optical biosensors.[12,27] However, little work on the use of anodic TiO_2 for optical sensing of condensable vapors has been reported: to the best of our knowledge, only one study, reported by us, has

Received: May 18, 2012
Accepted: July 18, 2012
Published: July 18, 2012

appeared.[28] Lately, by combining cold work of the metal foil and electrochemical anodization, we obtained a novel type of nanoporous TiO_2 consisting of interwoven nanotubes.[29]

This formulation demonstrated significantly improved photocatalytic efficiency compared to the more commonly studied nanotube arrays, although no detailed characterization of the response and the sensitivity of the anodic TiO_2 sensor element were given. In this work, based on this newly reported type of nanoporous TiO_2 structures, we systematically investigated vapor sensing and photocatalytic refreshing with three test analytes: isopropyl alcohol (IPA), dodecane and pentane. IPA, dodecane and pentane are commonly used in industry and are considered as toxic pollutants to the environment. To better monitor the air quality, sensors for detecting these three analytes have been widely investigated.[4,30,31] In our work, we find the nanoporous TiO_2 material to exhibit good sensitivity to the three organic vapors and reliable self-cleaning capability.

EXPERIMENTAL SECTION

Synthesis of Nanoporous TiO_2 Materials. Fabrication of nanoporous TiO_2 was carried out following the published method of Li, et al.[29] An industrial rolling mill (ONO 5″ Two High Rolling Mill Machine) with a rotary drum 125 mm in diameter was used to cold-work a Ti foil (Aldrich, 99.7% purity, 0.25 mm thick). A schematic diagram of the cold-rolling process is shown in Figure S1 (see the Supporting Information). The Ti substrate was fed into the rolling mill and repetitively rolled at a rolling speed of 8 revolutions per minute. The dimensions of the substrate were measured before and after cold-rolling, so that the percent of cold work (%CW), which measures the plastic deformation in the material, could be determined

$$\%\mathrm{CW} = \frac{A_0 - A_d}{A_0} \times 100\% \quad (1)$$

where A_o and A_d are the cross-sectional area of the foil before and after cold-work. Ti substrates were cold-worked to 56%CW.

The cold-worked Ti substrates were ultrasonically cleaned in acetone and ethanol successively and then dried in a nitrogen stream before anodization. Anodic TiO_2 films were generated in a two-electrode electrochemical cell, with a Pt gauze counter electrode and a Ti working anode. A press-contact to the back of the Ti working anode was made using Al foil, and the anode was sealed in the electrochemical cell by means of an elastomeric O-ring, which defined a working area of 1.2 cm^2. An ethylene glycol (99%+, Sigma-Aldrich) solution of 0.27 wt % NH_4F (98%+, Sigma-Aldrich) was used as the electrolyte. A computer-controlled Keithley 2400 Sourcemeter was used to apply the anodization voltage and record the anodization current simultaneously. The anodization experiments were carried out at 60 V for 40 min. The specimen was rinsed with ethanol and deionized (DI) water, and then dried in a nitrogen stream. The as-prepared nanoporous TiO_2 thin film was further annealed at 450 °C for 3 h in air before the sensing experiments.

Reflectometric Interference Fourier Transform Spectroscopy (RIFTS) Measurements. Optical characterization of the TiO_2 thin film was performed on the setup shown schematically in Figure 1 as previously described.[32] Reflectance spectra of the TiO_2 samples were acquired at normal incidence using a tungsten light source and a CCD spectrometer (USB 4000, Ocean Optics, inc.). The tungsten light source was focused through a microscope objective lens onto the film surface. Light reflected from the film was collected through the same microscope and recorded by a CCD detector in the wavelength range 400-1000 nm, with a spectral acquisition time of 300 ms and average spectral scans of 5. The reflectance spectrum was processed by Fast Fourier transform (FFT), which directly yields the value of nL of the film,[32] where n is the average refractive index of the porous layer and L is its physical thickness. The quantity nL is referred to as "effective optical thickness" in this work. The FFT spectrum was monitored in real-time to detect the changes in effective optical thickness throughout the vapor sensing experiments.

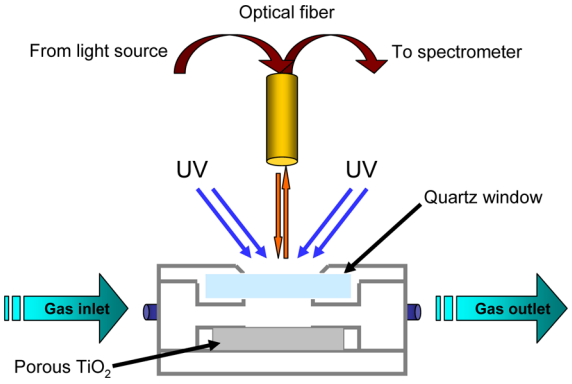

Figure 1. Schematic diagram of the vapor flow cell setup used in the sensing experiments.

Characterization Methods. Optical thickness and porosity were measured using the spectroscopic liquid infiltration method (SLIM),[32] in which reflectance spectra of the dry sample and of the sample immersed in ethanol were collected at the same spot. The shift of the film's effective optical thickness upon infiltration of ethanol is related to the porosity and the thickness of the film. A least-squares fit of the two effective optical thickness values and the refractive index values of air and ethanol was performed using the Bruggeman effective medium approximation, yielding the porosity and film thickness of the sample. The refractive index of the pure TiO_2 skeleton in the porous layer was determined to be 1.9 from this calculation.

Vapor Sensing. The TiO_2 sample was placed in a custom-made Teflon flow cell with an inlet connected to a gas mixer/mass flow controller. Organic vapors were generated by bubbling purified compressed air through a glass bubbler, which was immersed in a low-temperature water bath. The organic vapor-saturated air was then diluted to different concentrations by mixing with pure air. The total flow rate was maintained at 0.5 SLPM by mass flow controllers (Alicat Scientific). The sensing experiment was carried out at room temperature and the vapor concentrations were measured independently with either a photoionization detector (ppbRAE, RAE Systems) or a gas chromatograph equipped with a flame ionization detector (SRI 8610 C). After dosing, the analyte flow was changed to pure compressed air and UV illumination (λ_{max} = 365 nm) was passed through a quartz window to the surface of the sample (Fig. 1). The intensity of the UV light measured at the sample surface was ~17 mW/cm^2.

RESULTS AND DISCUSSION

For TiO_2-based optical gas sensors, the transduction methods of surface plasmon resonance transduction technique and optical waveguides have been reported.[33−35] Here, this study is based on applying nanoporous TiO_2 thin films as optical interferometric sensors.

Electrochemical anodization of the Ti foil resulted in porous layers approximately 2.5 micrometers in thickness and containing pores of average diameter 30 nm (Figure 2A, B). Scanning electron microscope (SEM) images revealed that the porous TiO_2 film was uniform, with tiny interwoven tubes primarily aligned perpendicular to the surface of the Ti metal foil. The porous TiO_2 layer was sufficiently smooth and flat that the reflectance spectrum displayed well-defined optical interference fringes (Figure 2C). These Fabry-Perot fringes originate from the interference of light reflecting from the air/film and film/substrate interfaces. The maximum of a given Fabry-Perot fringe observed at wavelength λ is determined by

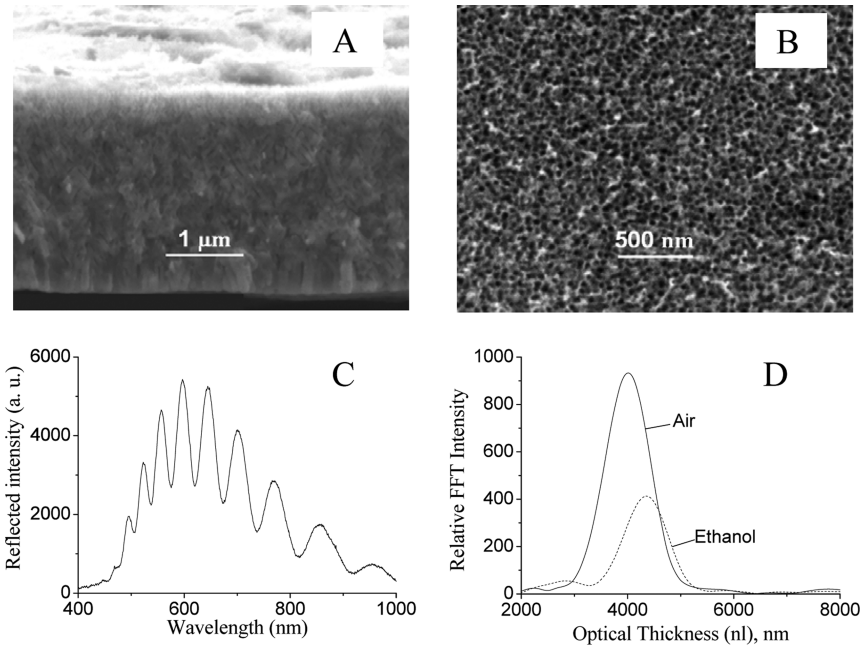

Figure 2. (A) Representative cross-sectional scanning electron microscope (SEM) image, (B) plan-view SEM image, (C) optical reflectivity spectrum, and (D) reflective interferometric Fourier transform spectrum in air (solid line) and ethanol (dashed line) of the nanoporous TiO_2 films used in the present work.

the film thickness, L, and the effective refractive index of the film, n, by eq 2

$$m\lambda = 2nL \tag{2}$$

where m is an integer corresponding to the spectral order of the Fabry-Perot fringe. On reflectivity spectra, the Fabry-Perot fringe takes the form of a group of reflectivity peaks located at a series of wavelengths, λ, with a corresponding series of spectral orders, m. Therefore, by measuring the wavelengths of different reflectivity peaks (i.e, the Fabry-Perot fringe) on the spectrum and assigning their spectral orders by mathematic calculation, one can obtain the film effective optical thickness, nL. In the present work, the means of measuring analytes captured in the thin porous TiO_2 films relies on this optical interferometric relationship (eq 2). When the film is exposed to an organic vapor, adsorption or condensation of the vapor in the pores results in an increase in the quantity nL from eq 2 and a red-shift of the Fabry-Perot fringes due to the larger index of refraction of the chemical substance relative to air. Measurement of the quantity nL is achieved in real-time by fast Fourier transform (FFT) of the reflectance spectrum (Figure 2D), which is commonly called Reflective Interferometric Fourier Transform Spectroscopy (RIFTS).[36,37] Binding curves for the organic vapor sensor are based on the analysis of the shift of the effective optical thickness calculated by the RIFTS method.

Introduction of liquid ethanol to the nanoporous TiO_2 film results in an increase in the effective optical thickness, corresponding to replacement of air (refractive index 1.00) with ethanol (refractive index 1.3611) in the pores of the film (Figure 2D). A least-squares fit of the two values of effective optical thicknesses (from air and ethanol measurements) to a two-component Bruggeman effective medium approximation yields a porosity of 29 ± 2%, and a physical thickness of 2430 ± 70 nm for the film. This method of determining film thickness and porosity is called the Spectroscopic Liquid Infiltration Method (SLIM).[32] The value of the film thickness calculated using the SLIM method agrees reasonably well within error with that measured by cross-sectional SEM.

In order to investigate the organic vapor sensing capability of the nanoporous TiO_2 interferometer, three organic analytes, dodecane, IPA and pentane, were tested. The refractive indexes and saturation vapor pressures (P_{sat}) for these analytes are given in Table 1. The sensing experiments were carried out with the TiO_2 interferometer film repeatedly dosed with organic vapors (diluted in dry air) and purged with dry air for several cycles.

Table 1. Physical Properties of Dodecane, Isopropanol, and Pentane at 298 K

	refractive index, n_D[a]	saturation vapor pressure, P_{sat} (Torr)
dodecane	1.422	0.134
isopropanol	1.377	45.0
pentane	1.358	512.54
water	1.334	23.76

[a]Measured at 589.3 nm.

On the basis of their saturation vapor pressures, dodecane is expected to condense most readily in the porous nanostructure, followed by IPA and then pentane. Thus the sensor should display the greatest sensitivity to dodecane and the least sensitivity to pentane. This expectation is corroborated by the data: to observe a comparable response (~0.3% change in effective optical thickness, nL) only 75 ppmv of dodecane is needed (Figure 3A), whereas 4300 ppmv of IPA is required (Figure 4A). The sensor is quite insensitive to pentane (Figure 5A); 11000 ppmv of pentane is required to obtain a ten-fold lower response (~0.03% change in effective optical thickness, nL). The response of the sensor to water vapor (Fig. 5B) is similar to and of the same magnitude as the response to IPA; introduction of 9% relative humidity (or 1400 ppmv water vapor) results in a percent change in effective optical thickness

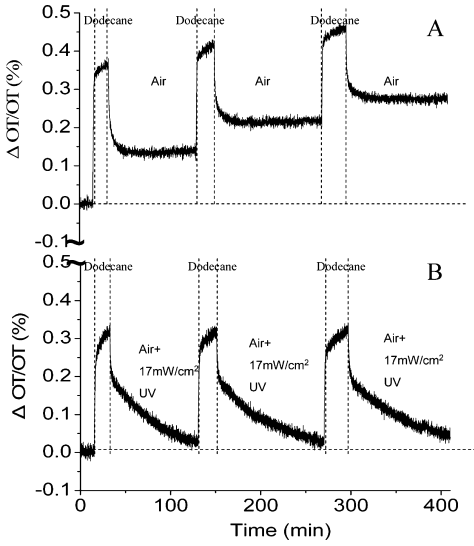

Figure 3. Dose-response curves of a nanoporous TiO_2 interferometer film repeatedly exposed to dodecane vapor (75 ppmv, diluted in air) and then purged with pure dry air, as indicated. (A) Normal sensor response (note the signal does not completely recover when the sensor is purged with pure air). (B) Sensor response when sample is exposed to UV (λ_{max} = 365 nm) illumination during the air purge steps. The quantity ΔOT/OT (%) is defined as $(nL_{final} - nL_{initial})/nL_{initial} \times 100\%$, where nL_{final} is the effective optical thickness (nL, as defined in eq 2) at time T, and $nL_{initial}$ is the effective optical thickness at time $T = 0$ prior to analyte exposure.

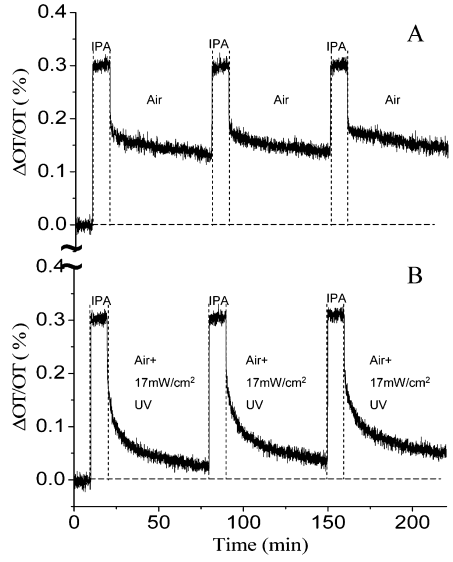

Figure 4. Dose-response curves of a nanoporous TiO_2 interferometer film repeatedly exposed to isopropanol vapor (4300 ppmv, diluted with air) and then purged with pure dry air, as indicated. (A) Normal sensor response. (B) Sensor response when sample is exposed to UV (λ_{max} = 365 nm) illumination during the air purge steps. The quantity ΔOT/OT (%) is defined as in Figure 3.

(nL) of ~0.2%. The detection limit of the nanoporous TiO_2 interferometer for dodecane and IPA was determined to be 2.5 and 30 ppmv, respectively (based on a signal-to-noise ratio of 2). In terms of sensitivity, the anodic nanoporous TiO_2 sensors reported here show a comparable sensitivity for IPA to the well-established porous silicon-based optical sensors.[4] It should be pointed out the sensors reported here have limited selectivity due to the fact that the sensing mechanism is based on detecting changes in the effective optical thickness of the films. However, the sensing selectivity can be potentially improved by surface modification of TiO_2, e.g., by tuning the surface hydrophobilicity, as suggested by other previous studies.[38]

The higher sensitivity seen for analytes of lower P_{sat} is consistent with the propensity of each analyte to remain in the condensed phase; analytes with smaller values of P_{sat}, have less tendency to desorb from the surface of the nanoporous TiO_2 sensor and so elicit a larger response. This property is also manifested in the rates of recovery of the sensor. For the experiments in which the sensor was exposed to repeated doses of dodecane, each successive air purge cycle was less effective than the last in recovering the baseline response (Figure 3A). The signal to noise (S/N) ratio also deteriorated after each sensing cycle. Thus the sensor was significantly poisoned after three dodecane/air cycles (Figure 3A). Poisoning of the porous TiO_2 interferometer sensor is attributed to build-up of residual dodecane in the pores of the nanostructure. Similarly, sensor poisoning was observed in the IPA sensing experiments: the original baseline signal could not be recovered even after purging with dry air for 1 h (Figure 4A). In contrast, the high P_{sat} value of pentane results in a low affinity for the TiO_2 surface; rapid and more nearly complete recovery of the signals was observed for this analyte (Figure 5A).

A noticeable difference in the dose-response curves of dodecane and IPA was observed (Figures 3A and 4A). In the case of dodecane, the baseline increased after each successive dose (Figures 3A), whereas with IPA, the baseline increased after the first dose, but then it remained at approximately the same level through subsequent doses (Figure 4A). This observed difference is attributed to two factors: (1) IPA forms hydrogen bonding interactions with the TiO_2 surface leading to a strongly adsorbed monolayer; and (2) IPA is less condensable than dodecane, such that multilayers of adsorbed IPA are more readily removed from the surface. Because of its strong preference for the condensed phase, dodecane is thought to continually infiltrate into the smaller micropores of the TiO_2 film after each dose. Even prolonged purges of >2 h were insufficient to remove dodecane from the TiO_2 sensor. By contrast, purge times of ~1 h were able to recover ~half of the baseline response to IPA. The reason that the signal did not return to the original baseline level but remained at a similar elevated level after each successive dose of IPA is attributed to a monolayer of IPA, strongly adsorbed via hydrogen bonding to the TiO_2 pore walls. Similar dose-recovery behavior was observed with water vapor exposures (Figure 5B), presumably due to analogous hydrogen bonding interactions between water and the TiO_2 pore walls.

The irreversible adsorption of low-volatility analytes is a particular problem with many point sensors, because it causes zero-point drift that can be unacceptable for environmental monitoring applications. Periodically or continuously heating the sensor to desorb or oxidatively degrade organic interferents has been successfully applied in optical,[4,39,40] capacitive,[41] or electronic (Taguchi-type)[42] chemical sensors, although this approach places limitations on the power requirements and physical properties of the sensor. The large bandgap of TiO_2 provides an alternative means to refresh the sensor element, based on photocatalytic oxidative degradation. This concept is well-established in the semiconductor photochemistry field, and the photocatalytic property of TiO_2 has been harnessed in self-disinfecting ceramics, self-cleaning windows, and waste treatment.[43,44] The photodegradation process usually involves an

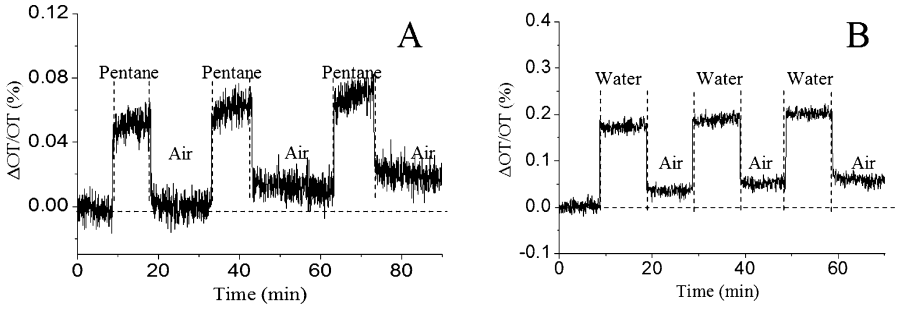

Figure 5. Dose-response curves of a nanoporous TiO_2 interferometer film repeatedly exposed to (A) pentane vapor (11000 ppm, diluted with air) or (B) water vapor (1400 ppmv, diluted with air) and then purged with pure dry air, as indicated. The quantity ΔOT/OT (%) is defined as in Fig. 3. Samples were not illuminated with UV light in these experiments.

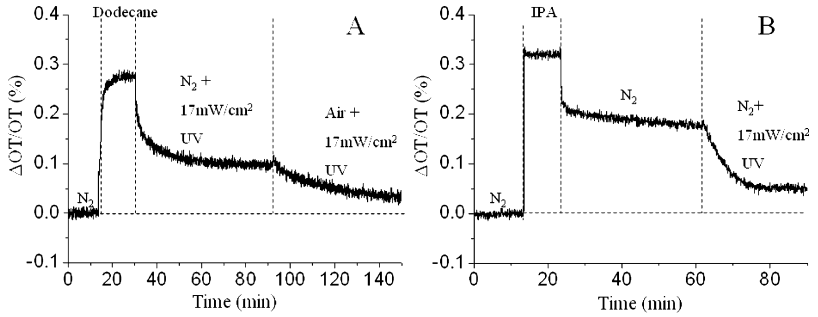

Figure 6. Effect of oxygen and UV light on the ability of the porous TiO_2 sensor to be refreshed. Dose-response curves of a nanoporous TiO_2 interferometer film exposed to (A) dodecane vapor (65 ppmv, diluted with pure dry nitrogen) or (B) IPA vapor (4300 ppm, diluted with pure dry nitrogen) and then purged with pure dry nitrogen (A) under UV irradiation, or (B) in the dark, as indicated. Dodecane requires both air and UV irradiation to display near-baseline recovery, whereas IPA can be substantially refreshed by UV exposure alone (in the absence of oxygen). The quantity ΔOT/OT (%) is defined as in Figure 3.

intermediate oxidant such as superoxide, hydroxyl radicals, peroxides, or singlet oxygen, and TiO_2 is the material of choice for many photooxidations because of its large band gap.[45] Photocatalytic degradation of organic species has also been discussed as a means to refresh optical biosensors constructed from TiO_2 films.[12,27] In this work, we investigated the effectiveness of photocatalytic degradation to refresh the vapor sensor after it has been exposed to a large dose of an organic analyte.

The self-cleaning photocatalytic oxidation process was carried out by illumination of the TiO_2 sensor with two UV lamps with maximal output at 365 nm, positioned as depicted in Figure 1. Samples were subjected to UV irradiation immediately after the air purge cycle was initiated. As seen in Figures 3B and 4B and Figure S2 in the Supporting Information, UV irradiation in the presence of air significantly improved the ability of the sensor to almost completely recover to its baseline value after exposure to either dodecane or IPA. Both the recovery time and the extent of recovery were improved by UV illumination. It should be pointed out that, considering that a hand-held UV lamp with low illumination intensity (17 mW/cm^2) was used in this study, it is highly possible that the measured long recovery time of the sensors studied here can be greatly shortened by using a high power UV lamp.

The photoreactions induced by TiO_2 destroy organics by converting them into volatile oxides such as CO_2 or NO.[7,8,43,46] Two of the more common photooxidation mechanisms invoked for TiO_2 systems involve conversion of water to a hydroxyl radical (•OH)[7,8] and conversion of molecular oxygen to singlet oxygen and superoxide species. Once formed, these highly reactive species then attack and degrade adsorbed organic materials. Although the chemical reaction is irreversible, the TiO_2 semiconductor is sufficiently stable that it can survive for many thousands of cycles without destruction of the underlying TiO_2 nanostructure.

To test for the involvement of oxygen in the current photolytic system, control experiments were performed in which the photoexcitation reaction was carried out in a dry N_2 atmosphere (Figure 6). A porous TiO_2 sensor poisoned with dodecane did not recover completely under these conditions, and the signal-time traces (Figure 6A) appeared similar to those obtained in the absence of UV excitation (Figure 3A). However, when the purge gas was changed from N_2 to dry air, the baseline displayed an additional drop, decreasing to a value close to the initial baseline level within 1 h (Figure 6A). The final baseline level (after the carrier gas was switched from N_2 to air, after 1h UV illumination) was similar to the baseline level observed when the carrier gas used throughout the experiment was air, after 1h of UV exposure (Figure 3B).

Exposure to UV light was also effective at removing IPA from the porous TiO_2 sensor. Similar to the response to dodecane, the sensor was poisoned by exposure to IPA vapor in N_2 (Figure 6B), and it could not be fully regenerated with a purge of pure N_2. However, in contrast to the dodecane results, the poisoned sensor showed significant recovery when UV illumination was switched on during the N_2 purge (Figure 6B). Considering the essential role of H_2O and O_2 in photocatalytic oxidation on TiO_2, the degradation of IPA with TiO_2 in pure N_2 is somewhat surprising. To the best of our knowledge, all previous reports of photocatalytic oxidation of IPA by TiO_2 have been carried out in air or in aqueous

solutions containing electron scavengers (e.g., Ag^+, Pt/H^+, or O_2) and the degradation mechanisms were assumed to be those discussed above.[47,48] We hypothesize that IPA is the source of hydroxyl radicals in the present case; hole transfer from photoexcited TiO_2 to IPA generates the hydroxyl radicals directly; and these radicals then induce further degradation of the organic species (eqs 3 and 4)

$$TiO_2 + h\nu \rightarrow h^+ + e^- \quad (3)$$

$$(CH_3)_2OH + h^+ \rightarrow \cdot OH + (CH_3)_2{}^+ \quad (4)$$

The samples in the present study were handled in laboratory air prior to introduction to the sensing flow cell, so it is possible that some residual water exists on the TiO_2 surface that contributes to the photooxidation process. As seen with dodecane, introduction of air enhances photooxidation, resulting in nearly complete recovery of the sensor to its original baseline state.

CONCLUSIONS

Nanoporous TiO_2 films synthesized by anodization display well-resolved optical interference fringes, which provide a sensitive measure of species adsorbed from the gas phase. The nanoporous TiO_2 interferometers are more sensitive to analytes with lower vapor pressures, and the time dependence of desorption of these analytes depends on both vapor pressure and on hydrogen bonding capability of the analyte. Some degree of irreversibility of the sensor is observed with all analytes; dodecane results in particularly poor reversibility because of its low vapor pressure. The photocatalytic property of TiO_2 can be harnessed to markedly improve the reversibility of these sensors, via a photooxidation process that requires the presence of both UV light and oxygen to provide maximal reversibility. The results show that nanoporous TiO_2 interferometers are a type of promising sensing material with self-recovery abilities for the effective detection of chemical vapors.

ASSOCIATED CONTENT

Supporting Information

A scheme showing the cold-rolling process and a supporting figure showing more sensing cycles for dodecane. This material is available free of charge via the Internet at http://pubs.acs.org/

AUTHOR INFORMATION

Corresponding Author

*E-mail: msailor@ucsd.edu (M.J.S.); yangli@cityu.edu.hk (Y.Y.L.).

Notes

The authors declare no competing financial interest.

ACKNOWLEDGMENTS

This work was supported by City University of Hong Kong (Projects 9667056 and 7002741) and by the U.S. National Science Foundation (Grant DMR-0806859). T.L.K. acknowledges the Natural Sciences and Engineering Research Council of Canada (NSERC) for a postdoctoral fellowship.

REFERENCES

(1) Orellana, G., *Frontiers in Chemical Sensors: Novel Principles and Techniques*; Springer-Verlag: Berlin, 2005.
(2) Ruminski, A. M.; Barillaro, G.; Chaffin, C.; Sailor, M. J. *Adv. Funct. Mater.* **2011**, *21*, 1511−1525.
(3) Fan, Z. Y.; Lu, J. G. *Appl. Phys. Lett.* **2005**, *86*, 123510.
(4) Kelly, T. L.; Gao, T.; Sailor, M. J. *Adv. Mater.* **2011**, *23*, 1776−1781.
(5) Li, C.; Zhang, D. H.; Liu, X. L.; Han, S.; Tang, T.; Han, J.; Zhou, C. W. *Appl. Phys. Lett.* **2003**, *82*, 1613−1615.
(6) Xiao, M. W.; Wang, L. S.; Wu, Y. D.; Huang, X. J.; Dang, Z. *J. Solid State Electrochem.* **2008**, *12*, 1159−1166.
(7) Gaya, U. I.; Abdullah, A. H. *J. Photochem. Photobiol., C* **2008**, *9*, 1−12.
(8) Fujishima, A.; Zhang, X. T.; Tryk, D. A. *Surf. Sci. Rep.* **2008**, *63*, 515−582.
(9) Chen, X. B.; Liu, L.; Yu, P. Y.; Mao, S. S. *Science* **2011**, *331*, 746−750.
(10) Liu, G.; Wang, L. Z.; Yang, H. G.; Cheng, H. M.; Lu, G. Q. *J. Mater. Chem.* **2009**, *20*, 831−843.
(11) Mor, G. K.; Varghese, O. K.; Paulose, M.; Grimes, C. A. *Sens. Lett.* **2003**, *1*, 42−46.
(12) Song, Y. Y.; Schmuki, P. *Electrochem. Commun.* **2010**, *12*, 579−582.
(13) Biskupski, D.; Herbig, B.; Schottner, G.; Moos, R. *Sens. Actuators, B* **2011**, *153*, 329−334.
(14) Wang, D. L.; Chen, A. T.; Jang, S. H.; Yip, H. L.; Jen, A. K. Y. *J. Mater. Chem.* **2011**, *21*, 7269−7273.
(15) Wang, Y. M.; Du, G. J.; Liu, H.; Liu, D.; Qin, S. B.; Wang, N.; Hu, C. G.; Tao, X. T.; Jiao, J.; Wang, J. Y.; Wang, Z. L. *Adv. Funct. Mater.* **2008**, *18*, 1131−1137.
(16) Varghese, O. K.; Gong, D. W.; Paulose, M.; Ong, K. G.; Dickey, E. C.; Grimes, C. A. *Adv. Mater.* **2003**, *15*, 624−627.
(17) Varghese, O. K.; Gong, D. W.; Paulose, M.; Ong, K. G.; Grimes, C. A. *Sens. Actuators, B* **2003**, *93*, 338−344.
(18) Ou, H. H.; Lo, S. L. *Sep. Purif. Technol.* **2007**, *58*, 179−191.
(19) Chen, X.; Mao, S. S. *Chem. Rev.* **2007**, *107*, 2891−2959.
(20) Bavykin, D. V.; Friedrich, J. M.; Walsh, F. C. *Adv. Mater.* **2006**, *18*, 2807−2824.
(21) Yue, L.; Gao, W.; Zhang, D. Y.; Guo, X. F.; Ding, W. P.; Chen, Y. *J. Amer. Chem. Soc.* **2006**, *128*, 11042−11043.
(22) Ghicov, A.; Schmuki, P. *Chem. Commun.* **2009**, 2791−2808.
(23) Grimes, C. A. *J. Mater. Chem.* **2007**, *17*, 1451−1457.
(24) Mor, G. K.; Shankar, K.; Paulose, M.; Varghese, O. K.; Grimes, C. A. *Nano Lett.* **2006**, *6*, 215−218.
(25) Song, Y. Y.; Schmidt-Stein, F.; Berger, S.; Schmuki, P. *Small* **2010**, *6*, 1180−1184.
(26) Ghicov, A.; Tsuchiya, H.; Hahn, R.; Macak, J. M.; Munoz, A. G.; Schmuki, P. *Electrochem. Commun.* **2006**, *8*, 528−532.
(27) Mun, K. S.; Alvarez, S. D.; Choi, W. Y.; Sailor, M. J. *ACS Nano* **2010**, *4*, 2070−2076.
(28) Cheng, J. W.; Tsang, C. K.; Cheng, H.; Liang, F. X.; Li, Y. Y. *Phys. Status Solidi A* **2011**, *208*, 1389−1393.
(29) Li, H.; Zheng, L. X.; Shu, S. W.; Cheng, H.; Li, Y. Y. *J. Electrochem. Soc.* **2011**, *158*, C346−C351.
(30) Aguirre, N. M.; Perez, L. M; Colin, J. A.; Buenrostro-Gonzalez, E. *Sensors* **2007**, *7*, 1954−1961.
(31) Barko, G.; Hlavay, J. *Talanta* **1997**, *44*, 2237−2245.
(32) Sailor, M. J., *Porous Silicon in Practice: Preparation, Characterization, And Applications*; Wiley-VCH: Weinheim, Germany, 2012.
(33) Manera, M. G.; Cozzoli, P. D.; Leo, G.; Curri, M. L.; Agostiano, A.; Vasanelli, L.; Rella, R. *Sens. Actuators, B* **2007**, *126*, 562−572.
(34) Manera, M. G.; Leo, G.; Curri, M. L.; Comparelli, R.; Rella, R.; Agostiano, A.; Vasanelli, L. *Sens. Actuators, B* **2006**, *115*, 365−373.
(35) Ohodnicki, P. R.; Wang, C. J.; Natesakhawat, S.; Baltrus, J. P.; Brown, T. D. *J. Appl. Phys.* **2012**, *111*, 064320.
(36) Pacholski, C.; Yu, C.; Miskelly, G. M.; Godin, D.; Sailor, M. J. *J. Am. Chem. Soc.* **2006**, *128*, 4250−4252.
(37) Pacholski, C.; Sartor, M.; Sailor, M. J.; Cunin, F.; Miskelly, G. M. *J. Am. Chem. Soc.* **2005**, *127*, 11636−11645.
(38) Ghicov, A.; Schmuki, P. *Chem. Commun.* **2009**, 2791−2808.

(39) King, B. H.; Wong, T.; Sailor, M. J. *Langmuir* **2011**, *27*, 8576−8585.
(40) De Stefano, L.; Rotiroti, L.; Rea, I.; Iodice, M.; Rendina, I. *J. Phys-Condens Mat.* **2007**, *19*, 395008.
(41) Bjorkqvist, M.; Paski, J.; Salonen, J.; Lehto, V. P. *Ieee Sens. J.* **2006**, *6*, 542−547.
(42) Faglia, G.; Comini, E.; Pardo, M.; Taroni, A.; Cardinali, G.; Nicoletti, S.; Sberveglieri, G. *Microsyst. Technol.* **1999**, *6*, 54−59.
(43) McCullagh, C.; Skillen, N.; Adams, M.; Robertson, P. K. J. *J. Chem. Technol. Biotechnol.* **2011**, *86*, 1002−1017.
(44) Roy, P.; Dey, T.; Lee, K.; Kim, D.; Fabry, B.; Schmuki, P. *J. Am. Chem. Soc.* **2010**, *132*, 7893−7895.
(45) Schwitzgebel, J.; Ekerdt, J. G.; Gerischer, H.; Heller, A. *J. Phys. Chem.* **1995**, *99*, 5633−5638.
(46) Zhao, J.; Yang, X. D. *Build. Environ.* **2003**, *38*, 645−654.
(47) Ohtani, B.; Nishimoto, S. *J. Phys. Chem.* **1993**, *97*, 920−926.
(48) Chavadej, S.; Phuaphromyod, P.; Gulari, E.; Rangsunvigit, P.; Sreethawong, T. *Chem. Eng. J.* **2008**, *137*, 489−495.